PHYSICAL REVIEW A **73**, 011803(R) (2006)

Controllable spontaneous decay at material wedges

S. C. Skipsey,[1] M. Al-Amri,[2] M. Babiker,[1] and G. Juzeliūnas[3]
[1]*Department of Physics, University of York, Heslington, York YO10 5DD, England*
[2]*Department of Physics,King Khalid Univeristy, P.O. Box 9003, Abha, Saudi Arabia*
[3]*Institute of Theoretical Physics and Astronomy of Vilnius University, A. Goštauto 12, 01108 Vilnius, Lithuania*
(Received 14 December 2005; published 19 January 2006)

We show that the de-excitation process of a dipole emitter can be altered controllably when it is embedded in a dielectric wedge of an arbitrary angle $0<\phi_0\leqslant 2\pi$. We focus here on the case of a dielectric wedge bounded by a perfect conductor and show that the de-excitation process for different wedges, distinguished by ϕ_0, displays a wide range of features. Besides the dependence on the emitter location at the narrow end, the de-excitation process exhibits a strong dipole orientational dependence, suggesting that the system might serve as a qubit in a controllable scalable hardware architecture for the purpose of quantum information processing.

DOI: 10.1103/PhysRevA.73.011803 PACS number(s): 42.50.Ct, 32.80.−t, 34.50.Dy, 41.20.Jb

There is currently a heightened research effort devoted to the important goal of identifying a qubit and a suitable environment that forms the basis for a scalable hardware architecture for the practical realization of quantum information processing [1]. A physical system that has recently been suggested as a candidate for such a purpose involves localized emitters in the form of atoms, molecules, or quantum dots embedded in a nanocrystal [2]. The suggestion was particularly persuasive as it followed the success of experiments performed by Grangier and co-workers who, for the first time, to the best of our knowledge, were able to demonstrate quantum cryptography using a nitrogen vacancy in a diamond nanocrystal as a single-photon source [3,4]. It has, however, been realized that a more versatile scenario could be achieved by making use of the interplay between dielectric cavity confinement and dipole orientation. Cavity confinement can control processes since it can lead to the enhancement and the complete suppression of the de-excitation process [5–8], with further control provided by the manipulation of the dipole orientation by optical means.

A different dielectric cavity QED system that we wish to highlight here, that seems promising for the purpose of quantum information processing, is the system in which a dipole emitter is localized near the sharp end of a material wedge. As far as the authors know, this quantum optical system has not been considered before, so its properties are hitherto unknown. The system, as shown schematically in Fig. 1, is a wedge-shaped dielectric slice of an arbitrary angle ϕ_0. The two planar surfaces of the wedge intersect along the z axis and are in contact with another material that, in general, could be another dielectric or a metal, but here we shall consider the case of a dielectric wedge bordered by a high conductivity metal, to be referred to as a perfect conductor. The dipole emitter is shown situated in the wedge region at the space point $\mathbf{R}=(x,y,0)=(\mathbf{r}_{\parallel},0)\equiv(r_{\parallel},\phi,0)$ in cylindrical polar coordinates, with the planar surfaces of the wedge defined by the equations $\phi=0$ and $\phi=\phi_0$.

The total Hamiltonian of the electromagnetic fields interacting with the emitter is given by

$$H=\hbar\omega_0\pi^{\dagger}\pi-\frac{1}{\varepsilon_0}\boldsymbol{\mu}\cdot\mathbf{D}(\mathbf{R})+H_f, \tag{1}$$

where $\mathbf{D}$ is the electric displacement operator of the field. The internal motion of the emitter is represented here in terms of only two states: $|e\rangle$, of energy E_e, and $|g\rangle$, of energy E_g, such that $E_e-E_g=\hbar\omega_0$, where ω_0 is the dipole excitation frequency. The operators π and $\pi^{\dagger}$ are lowering and raising operators for internal atomic states, so that $\boldsymbol{\mu}=\langle\boldsymbol{\mu}\rangle_{eg}(\pi+\pi^{\dagger})$ represents the dipole moment vector operator of the emitter. Here H_f is the quantized Hamiltonian of the electromagnetic fields in the dielectric region satisfying the boundary conditions at the conductor surfaces, namely, the vanishing of the components of the electric and magnetic fields tangential to the conductor surfaces. In the dielectric H_f has the usual form of expression as the sum of electric and magnetic energy densities integrated over all space and its quantization follows a standard path [9], the result of which is described below for the wedge geometry in question. The de-excitation rate for an excited emitter whose dipole moment vector is oriented in the direction $\hat{\boldsymbol{\mu}}$ is given by the golden rule:

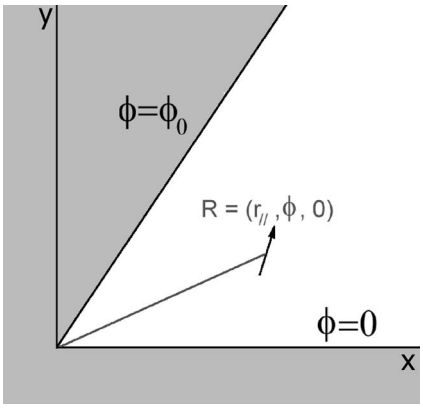

FIG. 1. Schematic drawing showing the dielectric wedge subtending an acute angle ϕ_0 in contact with a perfect conductor. The dipolar emitter is represented by the arrow positioned at the general point $\mathbf{R}$ of cylindrical coordinates $(r_{\parallel},\phi,0)$. The wedge interfaces are defined by the equations $\phi=0$ and $\phi=\phi_0$.

$$\Gamma_{\hat{\boldsymbol{\mu}}}(\mathbf{R}) = \frac{2\pi}{\hbar^2 \varepsilon_0^2} \sum_{Q} |\langle e;\{0\}| - \boldsymbol{\mu} \cdot \mathbf{D}(\mathbf{R}) |g;\{Q\}\rangle|^2 \delta(\omega(Q) - \omega_0), \tag{2}$$

where $|\{Q\}\rangle$ stands for a one-quantum state of the electromagnetic field satisfying the boundary conditions at the wedge surfaces; $\hbar\omega(Q)$ is the one-quantum energy and $|\{0\}\rangle$ stands for the electromagnetic vacuum field state. The quantized electric displacement field operator, **D** is evaluated at the position vector **R** of the emitter. The evaluation of the de-excitation rate requires the construction of the displacement field vector operator **D** in terms of field quanta satisfying electromagnetic boundary conditions at the wedge interfaces. For perfectly conducting boundaries the field modes emerge as either transverse electric TE, for which $E_z=0$, or transverse magnetic TM for which $B_z=0$. Using cylindrical coordinates $\mathbf{R}=(\mathbf{r}_\parallel, z)$ we write

$$\mathbf{D}(\mathbf{R}) = \sum_{\eta=1,2} \sum_{n} \int d^2\mathbf{k}_\parallel \{\boldsymbol{\mathcal{F}}^{(\eta)}_{\mathbf{k}_\parallel,n}(\mathbf{r}_\parallel, z, t) a_\eta(\mathbf{k}_\parallel, n) - \text{H.c.}\}, \tag{3}$$

where $\mathbf{k}_\parallel$ is a two-dimensional wave vector in the x-y plane. The operator $a_\eta(\mathbf{k}_\parallel, n)$ and its Hermitian conjugate are annihilation and creation operators for the quanta of the mode of polarization η, where η is either TE for which $\eta=1$, or TM, for which $\eta=2$. Their commutation rules are those for bosons

$$[a_\eta(\mathbf{k}_\parallel, n), a^\dagger_{\eta'}(\mathbf{k}'_\parallel, n')] = \delta_{\eta\eta'} \delta_{nn'} \delta(\mathbf{k}_\parallel - \mathbf{k}'_\parallel). \tag{4}$$

The vector functions $\boldsymbol{\mathcal{F}}^{(\eta)}_{\mathbf{k}_\parallel,n}(\mathbf{r}_\parallel, z, t)$ are the mode spatial distribution functions. For TE modes, $\eta=1$, the mode functions can be written as

$$\boldsymbol{\mathcal{F}}^{(1)}_{\mathbf{k}_\parallel,n}(\mathbf{r}_\parallel, z, t) = C_{k_\parallel,n} \left\{ J_m(k_\parallel r_\parallel) \frac{n\pi}{\phi_0} \sin\left(n\pi \frac{\phi}{\phi_0}\right) \frac{\hat{\mathbf{r}}_\parallel}{r_\parallel} - \frac{\partial J_m(k_\parallel r_\parallel)}{\partial r_\parallel} \cos\left(n\pi \frac{\phi}{\phi_0}\right) \hat{\boldsymbol{\phi}} \right\} e^{i[k_z z - \omega(k_\parallel, n)t]}, \tag{5}$$

where carets denote unit vectors and k_z is given by

$$k_z^2 = \varepsilon\omega^2/c^2 - k_\parallel^2 \tag{6}$$

with $\omega \equiv \omega(k_\parallel, n)$ being the mode frequency. In Eq. (5) and subsequently, $J_m(x)$ are Bessel functions, where m is related to integer $n \geqslant 0$ *b*

$$m = \frac{n\pi}{\phi_0}. \tag{7}$$

$C_{k_\parallel,n}$ are mode normalization factors given by

$$C_{k_\parallel,n} = \left(\frac{\hbar\omega}{2\pi\varepsilon\phi_0 k_\parallel^2} \right)^{1/2}. \tag{8}$$

For the TM mode ($\eta=2$) we have

$$\boldsymbol{\mathcal{F}}^{(2)}_{\mathbf{k}_\parallel,n}(\mathbf{r}_\parallel, z, t) = C_{k_\parallel,n} \left\{ \xi(k_\parallel) \frac{\partial J_m(k_\parallel r_\parallel)}{\partial r_\parallel} \sin\left(n\pi \frac{\phi}{\phi_0}\right) \hat{\mathbf{r}}_\parallel + \xi(k_\parallel) J_m(k_\parallel r_\parallel) \frac{n\pi}{\phi_0} \cos\left(n\pi \frac{\phi}{\phi_0}\right) \frac{\hat{\boldsymbol{\phi}}}{r_\parallel} + \frac{c k_\parallel^2}{\sqrt{\varepsilon}\omega} J_m(k_\parallel r_\parallel) \sin\left(n\pi \frac{\phi}{\phi_0}\right) \hat{\mathbf{z}} \right\} e^{i[k_z z - \omega(k_\parallel, n)t]}, \tag{9}$$

where

$$\xi(k_\parallel) = \left(1 - \frac{c^2 k_\parallel^2}{\varepsilon\omega^2}\right)^{1/2}. \tag{10}$$

The normalization of the fields has been carried out so that the electromagnetic field Hamiltonian H_f, described in the context of Eq. (1), reduces to the canonical form:

$$H_f = \frac{1}{2} \sum_{\eta=1,2} \sum_{n} \int d\mathbf{k}_\parallel \hbar\omega(k_\parallel, n) [a^\dagger_\eta(\mathbf{k}_\parallel, n) a_\eta(\mathbf{k}_\parallel, n) + a_\eta(\mathbf{k}_\parallel, n) a^\dagger_\eta(\mathbf{k}_\parallel, n)]. \tag{11}$$

This amounts to the condition

$$\int \boldsymbol{\mathcal{F}}^{(\eta)}_{\mathbf{k}_\parallel,n}(\mathbf{r}_\parallel, z, t) \cdot \boldsymbol{\mathcal{F}}^{(\eta)*}_{\mathbf{k}_\parallel,n}(\mathbf{r}_\parallel, z, t) d^2\mathbf{r}_\parallel dz = \tfrac{1}{2}\hbar\omega(k_\parallel, n), \tag{12}$$

where we have suppressed the subscript η in ω for the ease of notation.

The procedure for evaluating the de-excitation rate involves substituting from Eqs. (5) and (9) in Eq. (3) and subsequently in Eq. (2). It turns out that for a general angle ϕ_0 and after carrying out straightforward integrations, the ensuing expression for Γ cannot be reduced any further to a simple analytical form and, in general, the final steps in the evaluation inevitably involve some numerical analysis.

There are four different types of dielectric environments in which the emitter can be localized. These are distinguished by the range of the angle ϕ_0 as follows: (a) $0 < \phi_0 < \pi$, representing a dielectric wedge surrounded by a metal that occupies most of the space; (b) $\phi_0 = \pi$, representing a dielectric half-space in contact with a metallic half-space. This is the much discussed case of an emitter in front of a planar metallic surface [2,5–9]; (c) $\pi < \phi_0 < 2\pi$ in which the metallic region forms a wedge and the dielectric occupies most of the space; and, finally, (d) $\phi \approx 2\pi$ in which the conductor forms a sheet of infinitesimal thickness occupying the half-plane x-z embedded in a dielectric bulk. In this way, the wedge geometry accommodates a variety of situations ranging between a half metal plane and a full metal plane. It should be emphasized that all elements of our formalism, including the quantized fields defined above, are applicable to all these cases with ϕ_0 assuming any value within the continuous range between 0 and 2π. Throughout, the emitter is assumed to be localized in the dielectric at a well-defined position, which is considered to be controllably variable. It is possible to examine the manner in which the de-excitation rate distribution for emitters localized in the z

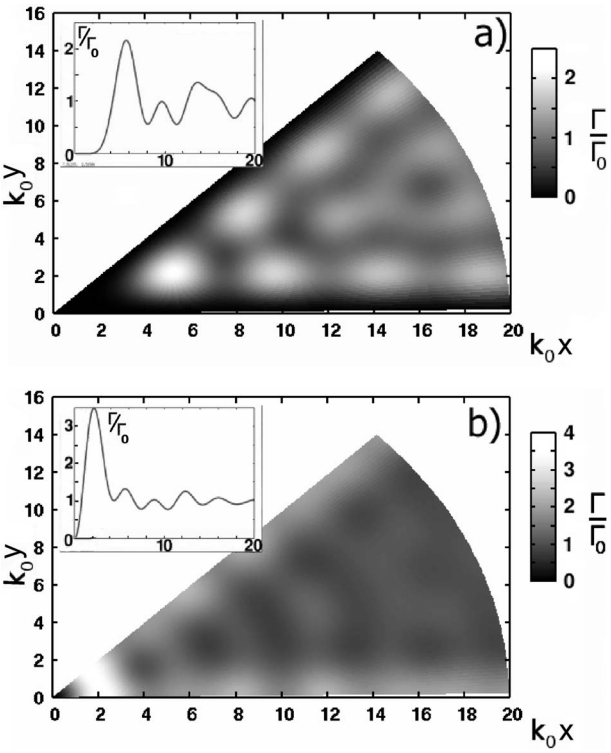

FIG. 2. Dielectric wedge for which $\phi_0=\pi/4$ embedded in a perfect conductor. The main figure shows the spatial distributions of the relative emission rate Γ/Γ_0 for dipole emitters in the x-y plane when the dipole moment is (a) oriented along the z axis (perpendicular case) and (b) oriented parallel to the x-y plane (along the azimuthal direction $\hat{\boldsymbol{\phi}}$). Distances are in units of k_0^{-1} where $k_0=\lambda_0/2\pi$, where λ_0 is the dipole transition wavelength. The brightest regions represent maximum emission rates. The inset for each case shows the variation of the corresponding relative rate at points along the symmetry line $\phi=\pi/8$.

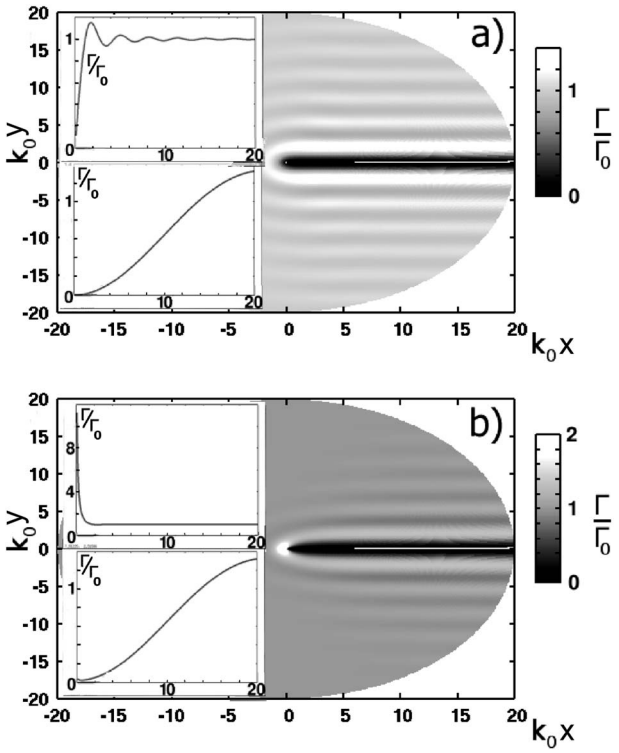

FIG. 3. Metallic half-plane embedded in a dielectric ($\phi_0\approx 2\pi$). Spatial distributions of the relative emission rate (referred to as Γ for convenience) for dipole emitters in the x-y plane when the dipole moment is (a) oriented along the z axis (perpendicular case) and (b) oriented in the x-y plane—along the radial direction $\hat{\mathbf{r}}_{\parallel}$. Distances are measured as in Fig. 2 and the brightest regions are regions of highest emission rates. The insets for each case show the variation of the corresponding relative rate at points along the symmetry line ($\phi=\pi$) in the upper inset, and along a line at $\phi=\pi/50$ in the lower.

$=0$ plane evolves with changing angle ϕ_0 in the different environment cases mentioned above. The results, displayed below, are in the form of gray scale graphs in which the rate is enhanced in certain regions (regions of super-radiance) continuously decreasing to regions where it is suppressed (regions of subradiance). The rate is normalized in terms of the rate Γ_0 in an infinite dielectric given by

$$\Gamma_0 = \frac{4\mu^2\omega_0^3}{3\pi\varepsilon_0 c^3\hbar}\mathcal{R}, \tag{13}$$

where $\mathcal{R}$ is a factor accounting for the local field corrections [10–13] and depends on ε, the relative permittivity of the dielectric in which the emitter is embedded. In Figs. 2(a) and 2(b) we should note the marked change in behavior when the dipole orientation is switched from perpendicular, i.e., along the edge (z axis) to being in-plane (i.e., in the x-y plane). Note also that in the parallel dipole orientation case, the region nearest to the narrow end of the wedge, Fig. 2(b), is a region of enhancement, while the corresponding region in the perpendicular dipole orientation is a region of high suppression. Excited emitters with perpendicular dipole orientations situated in this region, in principle, preserve their state of excitation indefinitely. In fact it can be seen that regions of enhancement in Fig. 2(a) correspond to regions of suppression in Fig. 2(b) and vice versa. If an emitter localized in a dark region is suddenly made to change its dipole orientation by optical means, for example, from parallel to perpendicular, the emitter could be de-excited at an enhanced rate, i.e., the emission changes from subradiant to super-radiant, depending on the location of the emitter. It is envisaged that this *in situ* control of de-excitation from subradiant to superradiant could be useful in quantum information processing. We have checked by explicit evaluation that the analytical framework for a general ϕ_0 reproduces the well-known results for the two types of dipole orientations for an emitter in front of a metallic half-space by setting $\phi_0=\pi$, which represents a useful check of the correctness of the procedure. Finally we should highlight the interesting extreme case of the general system we have defined, namely, the case in which the angle ϕ_0 becomes approximately equal to 2π. In this limit the dipole emitter is near a metallic half-plane occupying half the x-z plane, embedded in a full-space dielectric bulk. The results for the relative de-excitation rate Γ/Γ_0 are displayed in Fig. 3 for the two dipole orientations. It is seen that the rate varies symmetrically around the line of

termination (the positive x axis) for all excited emitters localized in the dielectric in the vicinity of the edge. We have checked by explicit evaluations that at sufficiently large distances from the termination line the de-excitation rate distributions on either side of the half-plane approach those appropriate for an emitter in front of a perfect conductor plane. This is clearly seen in Fig. 3(a). A change in the dipole orientation as seen in Fig. 3(b) modifies the rate distribution markedly, with considerable enhancement experienced in the vicinity of the termination line. As far as the authors know, this is the first time that a treatment of this kind for dipole decay near the termination line of a metallic half-plane has been put forward and so is of interest in its own right.

At very short distances of the emitters from the dielectric-conductor interfaces, one needs to modify the model to incorporate nonradiative losses due to finite conductivity and take account of surface roughness. In practice, one would seek to position the emitters in the vicinity of super-radiance or subradiance regions located at distances that are of the order of a significant fraction of a wavelength. For optical transitions, these are of the order of hundreds of nanometers from the interfaces and so, as a first approximation, any nonradiative (resistive) effects can be safely ignored.

In conclusion we have put forward a general framework that quantifies the de-excitation rate for dipolar emitters embedded in a wedge-shaped dielectric surrounded by high conductivity metal. The treatment is general in the sense that it is capable of predicting de-excitation rate distributions for the case of a wedge of an arbitrary angle ϕ_0 and we have highlighted the significance of the results in the limit of ϕ close to 2π, corresponding to dipole decay near the termination line of a metallic half-plane.

The prospect of the applicability of the work presented here to the area of quantum information processing rests in the suggestion that the de-excitation rate of dipole emitters near the narrow end of the wedge can be controlled optically from totally dark to super-radiant by a change of dipole orientation. Work is now in progress to explore the two-body and multibody cooperative effects in the same environment, since such effects are envisaged to be important for the realization of two-bit quantum gates [14–16]. The general situation differs considerably from the familiar problem of a pair of dipoles in front of a plane (corresponding to a specific case where $\phi_0=\pi$ in our analysis). For instance, if we have two dipoles at different points, one parallel and one perpendicular to one of the metal planes, the two dipoles are totally uncoupled through the field for $\phi_0=\pi$. However, in a more general situation, the pendicular and parallel dipoles would be coupled for all wedge angles with $\phi_0 \neq \pi$. This is just one transparent example of the uniqueness of the wedge case that makes its results quite distinct from the well-known single and parallel plane cases [17]. The processes of addressing and the readout of qubits are envisaged to be achievable in a similar manner to that for the situation in ion traps [18], but the solid state environment, for example, the case of color centered in a wedge-shaped nanocrystal, is clearly advantageous in terms of scalability. It would be particularly advantageous to exploit the absence of unwanted color center recoil in the processes of emission and absorption and the implications of this for the control of decoherence. The experimental realization of the system we suggest here is not expected to pose difficulties since any desired shape made with a variety of different materials can now be created, thanks to recent advances in material preparation at the nanoscale using modern deposition techniques and lithography. These advances, coupled with parallel advances in the detection of atomic and molecular position to nanometre accuracy [19] should make the predictions we have made here amenable to direct experimental investigation.

S.C.S. is grateful to the EPSRC for financial support. This work was partially funded by the Royal Society of London, supporting a visit by G.J. to the University of York.

[1] *The Physics of Quantum Information*, edited by D. Bouwmeester, A. Ekert, and A. Zeilinger (Springer, Berlin, 2000).

[2] M. Al-Amri and M. Babiker, Phys. Rev. A **67**, 043820 (2003); **69**, 065801 (2004).

[3] A. Beveratos, R. Brouri, T. Gacoin, J.-P. Poizat, and P. Grangier, Phys. Rev. A **64**, 061802(R) (2001).

[4] R. Brouri, A. Beveratos, J.-P. Poizat, and P. Grangier, Opt. Lett. **25**, 1294 (2000).

[5] E. A. Hinds, Adv. At., Mol., Opt. Phys. **28**, 237, (1990).

[6] *Cavity QED*, edited by P. Berman (Academic Press, San Diego, 1994).

[7] H. J. Kimble and T. W. Lynn, in *Coherence and Quantum Optics VIII*, edited by N. P. Bigelow, J. H. Eberly, C. R. Stroud, and I. A. Walmsley (Kluwer Academic, New York, 2003).

[8] S. Haroche, in *Cavity Quantum Electrodynamics*, edited by J. Dalibard, J. M. Raimond, and J. Zinn Justin, Fundamental Systems in Quantum Optics, Les Houches, Session LIII (Elsevier Science Publishers, New York, 1992).

[9] E. A. Power and T. Thirunamachandran, Phys. Rev. A **25**, 2473 (1982).

[10] R. J. Glauber and M. Lewenstein, Phys. Rev. A **43**, 467 (1991).

[11] S. M. Barnett, in *Quantum Fluctuations*, edited by S. Reynaud, E. Giacobino, and Zinn-Justin, Les Houches Lectures, Session 62 (Elsevier, Amsterdam, 1997).

[12] P. de Vries and A. Lagendijk, Phys. Rev. Lett. **81**, 1381 (1998).

[13] G. Juzeliūnas and D. L. Andrews, Adv. Chem. Phys. **112**, 357 (2000).

[14] D. Jaksch, J. I. Cirac, P. Zoller, S. L. Rolston, R. Cote, and M. D. Lukin, Phys. Rev. Lett. **85**, 2208 (2000).

[15] T. Calarco, A. Datta, P. Fedichev, E. Pazy, and P. Zoller, Phys. Rev. A **68**, 012310 (2003).

[16] U. Dorner, P. Fedichev, D. Jaksch, M. Lewenstein, and P. Zoller, Phys. Rev. Lett. **91**, 073601 (2003).

[17] T. Kobayashi, Q. Zheng, and T. Sekiguchi, Phys. Rev. A **52**, 2835 (1995).

[18] H. C. Nägerl *et al.*, in *The Physics of Quantum Information* (Ref. [1]), p.163.

[19] J. Michaelis, C. Hettish, J. Mlynek, and V. Sandoghdar, Nature **405**, 325 (2000).